Quantitative Phosphoproteomics Reveals Wee1 Kinase as a Therapeutic Target in a Model of Proneural Glioblastoma

Citation: Lescarbeau, Rebecca S. et al. "Quantitative Phosphoproteomics Reveals Wee1 Kinase as a Therapeutic Target in a Model of Proneural Glioblastoma." Molecular Cancer Therapeutics 15, 6 (March 2016): 1332–1343 © 2016 American Association for Cancer Research

As Published: http://dx.doi.org/10.1158/1535-7163.MCT-15-0692

Publisher: American Association for Cancer Research (AACR)

Persistent URL: http://hdl.handle.net/1721.1/117725

Version: Author's final manuscript: final author's manuscript post peer review, without publisher's formatting or copy editing

Published in final edited form as:

Mol Cancer Ther. 2016 June ; 15(6): 1332–1343. doi:10.1158/1535-7163.MCT-15-0692-T.

Quantitative phosphoproteomics reveals Wee1 kinase as a therapeutic target in a model of proneural glioblastoma

Rebecca S. Lescarbeau[1], **Liang Lei**[2], **Katrina K. Bakken**[3], **Peter A. Sims**[4], **Jann N. Sarkaria**[3], **Peter Canoll**[2], and **Forest M. White**[1,‡]

[1]Department of Biological Engineering and David H. Koch Institute for Integrative Cancer Research, Massachusetts Institute of Technology, Cambridge, Massachusetts

[2]Department of Pathology and Cell Biology and Herbert Irving Comprehensive Cancer Center, Columbia University, New York, New York

[3]Department of Radiation Oncology, Mayo Clinic, Rochester, Minnesota

[4]Department of Systems Biology and Department of Biochemistry and Molecular Biophysics, Columbia University, New York, New York

Abstract

Glioblastoma (GBM) is the most common malignant primary brain cancer. With a median survival of about a year, new approaches to treating this disease are necessary. To identify signaling molecules regulating GBM progression in a genetically engineered murine model of proneural GBM, we quantified phosphotyrosine mediated signaling using mass spectrometry. Oncogenic signals, including phosphorylated ERK MAPK, PI3K, and PDGFR, were found to be increased in the murine tumors relative to brain. Phosphorylation of CDK1 pY15, associated with the G_2 arrest checkpoint, was identified as the most differentially phosphorylated site, with a 14-fold increase in phosphorylation in the tumors. To assess the role of this checkpoint as a potential therapeutic target, syngeneic primary cell lines derived from these tumors were treated with MK-1775, an inhibitor of Wee1, the kinase responsible for CDK1 Y15 phosphorylation. MK-1775 treatment led to mitotic catastrophe, as defined by increased DNA damage and cell death by apoptosis. To assess the extensibility of targeting Wee1/CDK1 in GBM, patient-derived xenograft (PDX) cell lines were also treated with MK-1775. Although the response was more heterogeneous, on-target Wee1 inhibition led to decreased CDK1 Y15 phosphorylation and increased DNA damage and apoptosis in each line. These results were also validated *in vivo*, where single-agent MK-1775 demonstrated an anti-tumor effect on a flank PDX tumor model, increasing mouse survival by 1.74-fold. This study highlights the ability of unbiased quantitative phosphoproteomics to reveal therapeutic targets in tumor models, and the potential for Wee1 inhibition as a treatment approach in pre-clinical models of GBM.

‡**Corresponding Author:** Forest White. Address: 77 Massachusetts Avenue, 76-353F, Cambridge, MA 02139, ; Email: fwhite@mit.edu

Conflicts of Interest: The authors disclose no potential conflicts of interest.

Keywords

Glioblastoma; Signaling; Wee1; Mass spectrometry

INTRODUCTION

Glioblastoma (GBM), grade IV astrocytoma, is one of the most devastating cancers, with a 1 year survival rate of 35% and a 5 year survival rate of only 4.7% ([1]). The current standard of care includes surgical resection, radiation, and temozolomide ([2]). GBM tumors are infiltrative and invade the parenchyma, often necessitating multiple surgeries and making full resection nearly impossible ([3]). Despite improvements associated with targeted therapeutics in many other cancer types, effective novel therapeutic strategies leading to improved survival have not been realized in GBM. Therefore, there is a clear unmet need to identify new GBM therapeutic strategies.

Genomic profiling of over 500 human GBM tumor specimens by The Cancer Genome Atlas (TCGA) ([4], [5]) investigated gene expression, DNA copy number, nucleotide sequence aberration, and DNA methylation aberration data in these tumors. Somatic alterations were measured in the majority of tumors across multiple oncogenic pathways. Rates of copy number and sequencing alterations in the TP53, RB, and receptor tyrosine kinase (RTK) pathways were measured as 78%, 87%, and 88%, respectively, demonstrating the importance of these altered functional pathways. Specifically, 45% of GBMs analyzed had epidermal growth factor receptor (EGFR) mutations or significant copy number variations, and 13% had PDGFR alpha (PDGFRA) amplifications. Through RTKs, cells interact with growth factors and cell-cell interacting ligands that transmit external signals into the cell via tyrosine phosphorylation cascades that can affect cell morphology, function, growth, division, and survival. From the TCGA analysis, four robust and statistically significantly distinct GBM subtypes were identified: proneural, neural, classical, and mesenchymal ([6]). Each subtype has unique defining genetic aberrations and increased gene expression. Variation across these tumor subtypes have highlighted the complexity of this disease, as has a recent manuscript that describes the intra-tumoral cellular heterogeneity ([7]). In addition to the DNA aberrations and genetic expression differences, studying the signaling cascades and the effects of alterations in their RTK pathways will provide another layer of information to help understand and treat this disease.

Although genetic aberrations and mutations occur, cancer cells still must maintain a functional genome. If DNA damage is incurred, the cells must either initiate repair pathways to survive, or undergo apoptosis. To aid in this decision process, cell cycle transitions are dependent upon checkpoint complexes that are composed of cyclin dependent kinases (CDKs) and cyclins that are tightly controlled by positive and negative effectors, such as P53. P53 aberrations put additional stress on the other gate keepers to insure survival ([8–10]). These cell cycle checkpoints are of extreme importance because their loss can lead to reduced cellular fidelity and chromosomal abnormalities.

To understand how molecular alterations associated with GBM affect cellular signaling networks, we have investigated a genetically engineered murine model of proneural GBM

([11]). To identify potential therapeutic targets, we quantified tyrosine phosphorylation mediated signaling networks in tumors relative to those of normal brain tissues by mass spectrometry (MS). Proneural GBM murine tumors had increased signaling in oncogenic pathways, including increased phosphorylation on PDGFR, ERK 1/2 MAP kinases, and the PI3K/Akt signaling cascade. We also identified strongly increased phosphorylation on CDK1 Y15, a cell cycle inhibitory phosphorylation site, in these rapidly growing tumors. Inhibition of the upstream kinase with MK-1775, a Wee1 kinase inhibitor, abrogated phosphorylation of this site and caused mitotic catastrophe as measured by increased DNA damage, apoptosis, and decreased cell numbers in primary cell lines derived from these murine tumors. These results were substantiated in several GBM patient-derived xenograft (PDX) cell lines in vitro. Finally, in vivo treatment of flank human GBM PDX tumors with single-agent MK-1775 led to decreased phosphorylation of CDK1, increased DNA damage, and an anti-tumor effect.

MATERIALS AND METHODS

Murine Proneural GBM Tumor Model

The experimental procedures involving mice here were approved by the Institutional Animal Care and Use Committee (IACUC) of Columbia University and performed in accordance with institutional policies. Tumor induction was as described ([11]). Briefly, VSV-G pseudotyped PDGF-IRES-Cre (PIC) retrovirus was injected into the subcortical white matter of the right frontal hemisphere of adult mouse brains using a stereotaxis platform with a Hamilton syringe. The injection coordinates were 2.1 mm lateral, 2.2 mm rostral, and 1.8 mm deep with bregma as the reference point. The transgenic mice harbor floxed tumor suppressors Pten and Tp53, in addition to stop-floxed reporters YFP or Luciferase. All injections were done in mice between six and eight weeks of age. At first signs of tumor morbidity the frontal quadrant of the right cerebral hemisphere, which included the tumor and surrounding infiltrated brain tissue, were harvested and immediately frozen in liquid nitrogen. The control brains were collected similarly.

GBM PDX Tumor Model

Studies were approved by Mayo IACUC. Xenografts GBM6, GBM36, and GBM 38 were established in athymic mice (Harlan) as previously described ([12]). Briefly, xenografts and cell line models were established from resected tumor tissue of patients with GBM, descriptions in Table 1 ([12, 13]). Athymic female mice were inoculated subcutaneously with 2E6 cells. When tumors reached 200–350 mm^3 (long-duration study) or 500 mm^3 (short-duration study), mice were randomized to daily treatment via oral gavage with vehicle control (0.5% methoxycellulose) or MK-1775. Doses were delivered twice daily Monday-Friday and once daily on weekends. Flank tumors were measured thrice weekly, and mice were euthanized after 5 days of twice daily dosing (100 mg/kg, short-duration study) or when tumor volume exceeded 1500 mm^3 on two separate measurements or 2000 mm^3 (75 mg/kg, long-duration study).

Tumor Homogenization

Once excised, flash frozen tumors and brain tissues to be analyzed by MS and western blotting were homogenized (Polytron) in ice-cold lysis buffer consisting of 8M urea supplemented with 1 mM sodium orthovanadate, 0.1% Nonident P-40 (NP-40), and protease inhibitor and phosSTOP tablets (Roche), as described by Johnson and White ([14]). Samples were homogenized on ice using 5×10 sec pulses, with 10 sec intervening periods to prevent tissue heating. Protein concentrations were quantified by a bicinchoninic acid (BCA) assay (Pierce).

Mass Spectrometry Preparation

Homogenized tumor and brain samples were reduced in 10 mM DTT at 56°C for 45 min and alkylated with 50 mM iodoacetamide at room temperature for 1 hour in the dark, as described previously ([15]). Proteins were digested to peptides with sequencing grade trypsin (Promega) at 1:100 enzyme/substrate ratio at room temperature overnight in 100 mM ammonium acetate, pH 8.9. Trypsin activity was then quenched with acetic acid at a final concentration of 10%. Urea was removed by reverse-phase desalting using C18 cartridges (Waters). Samples were then lyophilized and stored at −80°C.

iTRAQ Labeling, Phosphotyrosine Enrichment, and MS Analysis

Peptides were labeled with iTRAQ 8plex isobaric mass tags (iTRAQ, AB Sciex) ([16]). Labeled, phosphotyrosine peptides were enriched by immunoprecipitation (IP) with a cocktail of three anti-phosphotyrosine antibodies followed by immobilized metal affinity chromatography (IMAC), as previously described ([17]). Briefly, 60 µL of protein G-agarose (EMD Millipore) beads were incubated with 12 µg pY100 (Cell Signaling Technologies, CST), 12 µg PT66 (Sigma), and 12 µg 4G10 (EMD Millipore) antibodies. Resuspended iTRAQ-labeled peptides were incubated with the antibody-conjugated protein G-agarose beads. Peptides were eluted from the antibody conjugation and further enriched using an IMAC column. The retained peptides were loaded onto a C18 pre-column, separated by reverse-phase HPLC (Agilent) over a 130 minute gradient, and injected into either an Orbitrap Elite or Q Exactive mass spectrometer (Thermo Scientific) using a custom ultra-low-flow nano-electrospray interface.

Phosphotyrosine Data Analysis

After conversion, mass spectra data files were searched against the National Center for Biotechnology Information Uniprot 2009 database containing *Mus musculus* protein sequences using Mascot 2.1.03 (Matrix Science) or SwissProt 2015_1 using Mascot 2.4.1. Precursor ion and MS/MS spectra information containing sequence and iTRAQ quantification data were extracted using CAMV ([18]). MS/MS spectra were manually validated to remove spectra containing contamination within the precursor isolation window and to ensure peptide sequence and phosphorylation site localization with the aid of CAMV ([18]). iTRAQ quantification data were corrected for isotopic overlap. Phosphotyrosine peptide iTRAQ ratios were normalized to mean relative protein quantification ratios obtained from the total protein of each iTRAQ channel.

Cell Culture

Primary cell lines (MGPP6 and MGPP7) derived from PTEN/P53-deleted proneural GBM murine tumors (described above) were cultured at 37°C and 5% CO2 in Dulbecco's Modified of Eagle's Medium with 4.5 g/L glucose, L-glutamine, and sodium pyruvate (DMEM, Corning), supplemented with 0.5% FBS, 1× Antibiotic-Antimycotic (Anti-Anti, Gibco), 1× N2 Supplement (Gibco), 20 μg/L 3,3',5-Triiodo-L-thyronine (Sigma), 10 ng/mL PDGF-AA (Peprotech), and 10 ng/mL FGF-Basic (Peprotech). MGPP6 and MGPP7 cells were plated on poly-L-lysine coated plates. PDX cell lines (GBM6, GBM36, and GBM38) were cultured at 37°C and 5% CO2 in DMEM media supplemented with 20% FBS and 1× Penicillin-Streptomycin (Pen-Strep, Gibco) as described previously ([19]).

Cell Counts

Primary and PDX cells were plated and allowed to adhere to plates overnight. The media was then replaced with media containing the indicated MK-1775 (Selleckchem) concentration and the cells were allowed to grow for an additional 48 hours. Cells were then counted using a cellometer (Nexcelom) and the cell counts were normalized to the number of cells grown in media without MK-1775.

Western Blots and Flow Cytometry

Prior to treatment with DMSO, MK-1775, or roscovitine (Selleckchem), primary and PDX cells were grown in their respective media overnight, then the media was replaced with media containing 1 μM MK-1775, 10 μM roscovitine, both inhibitors, or DMSO for the indicated time period. For western blotting, cells were lysed in 1× RIPA buffer (Boston Bioproducts) supplemented with 1× Halt Protease and Phosphatase Inhibitor Cocktail (Thermo Scientific) and 0.1 mM phenylmethanesulfonyl fluoride (Sigma). The lysates were cleared through centrifugation at 10,000g for 15 min. Protein concentrations were quantified by BCA assay. Western blots were developed on film using SuperSignal West Pico Chemiluminescent Substrate kit (Thermo Scientific). Quantification was performed using ImageJ 1.48V (National Institutes of Health). Anti-PTEN, anti-P53, and anti-CDK1 were purchased from Millipore, Calbiochem, and BD Bioscioences, respectively. Anti-pCDK1 (pY15), anti-β-tubulin, anti-γH2AX (pS139), and anti-GAPDH were purchased from CST. For flow cytometry, cells were washed, fixed in formaldehyde for 15 min at room temperature, and permeabilized and stored in methanol at −20°C. Fixed cells were incubated with anti-cleaved Caspase-3 (BD Biosciences) and anti-cleaved PARP (BD Biosciences) or anti- γH2AX (pS139) (Millipore) primary antibodies then with PE-conjugated goat anti-rabbit (Molecular Probes, Invitrogen) and Alexa Fluor 647-conjugated goat anti-mouse (Molecular Probes, Invitrogen) secondary antibodies. Cells were stained with 1.2 μg/mL Hoechst (Molecular Probes, Invitrogen). Samples were analyzed using a BD LSR II HTS Flow Cytometer (BD Bioscience) and the data were analyzed using FlowJo (V10, Tree Star). Flow cytometry events were acquired ungated, and live cell gates were created based on their forward and side light scatter profiles using FlowJo.

Computational Deconvolution to Determine Cell Type-specific Expression Patterns from RNA-seq Data

RNA-seq data from normal mouse brain (n=6) and the murine PTEN/P53-deleted proneural glioma model (n=7) was previously described ([20]), and has been deposited (SRA number SRP035462). Computational deconvolution was performed as previously described ([21, 22]) using the lineage marker genes Gfap, Olig2, Mog, Aif1, and Rbfox3.

Statistical Analysis and Bioinformatics

Data is expressed as mean and standard deviation of 3 or more experiments. For experiments in which two groups are compared, statistical analysis was performed using Student *t* test in Microsoft Excel 2010 or log-rank in Prism 5.03 (GraphPad). Statistical significance was defined as $p \leq 0.05$. Hierarchical clustering was performed using Matlab R2013b, 8.2.0.701 (Mathworks) with a Spearman correlation distance metric ([23]).

RESULTS

Characterization of Proneural GBM Murine Tumor Signaling Relative to Normal Brain

With the goal of characterizing signaling network alterations associated with the proneural subtype of GBM, we have utilized a genetically engineered mouse model of proneural GBM in which mice floxed for *Pten* and *Tp53* are stereotactically injected with a retrovirus expressing PIC. Tumors developed in this model therefore lack P53 and PTEN and overexpress PDGF, creating a molecular signature similar to that of human proneural GBM ([11, 20]). To quantify cellular signaling network alterations in these tumors, tyrosine phosphorylation profiles in tumors and brain tissue from non-injected mice were analyzed by quantitative MS. At sacrifice, tissues were excised and immediately flash frozen in liquid nitrogen. Frozen tissues were homogenized and their proteins were reduced, alkylated, and digested with trypsin to peptides. Peptides from each sample were differentially labeled with iTRAQ and phosphotyrosine-containing peptides were enriched using IP and IMAC prior to LC-MS/MS analysis for identification and quantification, Figure 1. A total of 249 phosphotyrosine (pTyr/pY) containing peptides from 185 proteins were identified and quantified in the first tumor cohort, consisting of seven tumors, for which the average mouse survival time was 39 days post-injection (DPI), and one brain tissue specimen (full quantitative data, including phosphorylation site localization can be found in Supplementary Table S1 and Supplementary Figure S1). In a separate analysis to assess the inherent variability in phosphotyrosine signaling across 8 mouse brain tissue specimens, 276 pTyr sites on 201 proteins were identified and quantified. To enable cross-analysis quantitative comparisons, the same normal brain tissue was included in all analyses as a normalization control. After normalizing the iTRAQ quantification of the phosphorylation sites to the brain control and log2 transforming the data, hierarchical clustering was performed on the 125 phosphosites present in the analysis of the first cohort and the normal brain tissues, Figure 2A and Supplementary Figure S2. As can be seen from the clustering results, tumor samples cluster together and separate from the brain samples, indicating that the overall signaling in tumors is distinct from normal biological signaling in the brain.

To validate the quantitative results from this analysis, a separate cohort of seven tumors (average survival time: 25 DPI) were analyzed relative to the same brain control. In total from replicate analyses of this cohort, 212 pTyr sites on 176 proteins were identified and quantified. When comparing the second tumor cohort to the normal brain specimens using the 78 phosphorylation sites identified in both analyses, the tumors again cluster together and separate from the brain samples, Supplementary Figure S3.

In addition to general separation of tumors from normal brain using their phosphorylation levels, phosphorylation signals characteristic of the PDGF-driven proneural mouse model were identified. Phosphorylation of an activating site on PDGFRα, pY742 ([24]), was increased by two-fold, on average, in tumors, Figure 2B. Correspondingly, phosphorylation of PI3K subunit P85 ([25]) and the activation loops of MAPK cascade ERK1/2 proteins ([26], [27]) downstream of PDGFR were also increased in tumors, Figure 2B. Interestingly, most of the sites identified in tumors and normal brains had increased phosphorylation in the brain tissues compared to the tumors, Figure 2A. For instance, phosphorylation of multiple sites on the Eph receptors was decreased in the tumors, consistent with either decreased cell-cell contact ([28]) in the diffusively invasive tumors or with altered cellular composition in the tumors compared to brain. Additionally, neuronal proteins, including glutamate receptors (Grin2A and Grin2B) and Dlg proteins, had decreased phosphorylation in the tumors, again consistent with a change in cellular compostion from a predominance of active neurons in the normal brain to a predominance of Olig2+ glioma cells in the proneural tumors, Figure 2C.

To further address the issue of the heterogeneous cellular composition, and to gain further insight into the cell type-specific alterations in the phosphotyrosine signature, we performed computational deconvolution analysis, as previously described ([20]–[22]) on RNA-Seq data from normal adult mouse brain (n=6) and endstage proneural mouse tumors (n=7). We then queried the results of the deconvolution analysis to assess the cell type-specific expression pattern of genes that showed alterations in phosphotyrosine levels in our iTRAQ data (Supplementary Table 1). Notably, several of the genes that showed alterations in phosphorylation were predominantly or exclusively expressed in one of the 5 cell types. For example, deconvolution analysis of RNA-Seq showed that glutamate receptors (Gran2A and Grin2B), and several synaptic genes (Dlg2, Syt1, Stx1a) are predominantly or exclusively expressed in neurons, while several kinases and cell cycle regulators (dyrk4, Cdk1, Cdk2, Fyn, and PDGFRa) are predominantly or exclusively expressed in olig2+ cells.

One of the most significantly increased phosphorylation sites in the tumor relative to the normal brain was on CDK1/2, with a 14-fold increase of the singly (tyrosine 15) and 6-fold increase of doubly (threonine (T) 14 and tyrosine 15) phosphorylated peptides, Figure 3A. Phosphorylation of these sites was low enough in the normal brain that they were not detected in the untargeted MS analysis of the 8 normal brain samples, which was dominated by signaling due to normal brain function. Thus, MS quantification for these peptides was based on the comparison between the brain normalization channel and the tumors in Cohort 1 or 2. Additionally, due to the inherent variability in identifications during non-targeted MS analysis, the doubly phosphorylated peptide was only detected in Cohort 1. The sequence of CDK1 and CDK2 are identical in the region surrounding these phosphorylation sites, and

therefore phosphorylation at T14 and Y15 on CDK1 or CDK2 are indistinguishable by either MS or western blot. For simplicity, we will refer to this site as CDK1 Y15, although it is possible that there is contribution from CDK1, CDK2, or both. Western blots were performed with antibodies recognizing CDK1 and phospho-CDK1/2 (Y15), Figure 3B. These blots demonstrate a significant (p=3.4E-4) increase in protein expression and confirm the significant (p=9.3E-4) increase in phosphorylation.

CDK1 Phosphorylation Reduced after Wee1 Kinase Inhibition

Increased phosphorylation on CDK1 Y15 in the tumor samples was initially unexpected because phosphorylation of this site causes cell cycle inhibition and delays cell cycle progression in the context of DNA damage ([29]), and yet the tumor cells were rapidly proliferating in this mouse model ([11]). Given the role of this phosphorylation site as a cell cycle checkpoint, we reasoned that inhibition of Wee1, the kinase responsible for phosphorylation of this site, might lead to premature cell cycle progression with unrepaired DNA damage and potentially to mitotic catastrophe in these cells. To test this hypothesis, we treated syngeneic primary cell lines MGPP6 and MGPP7 (P53- and PTEN-deficient, Supplementary Figure S4A), developed from the same tumor model, with the Wee1 inhibitor MK-1775 and observed a significant dose dependent decrease ($p<0.05$ at 0.1 μM for MGPP6 and 0.3 μM for MGPP7) in cell number after 48 hours of treatment, Figure 3C. At 1 μM MK-1775 treatment, the cell counts were 17.8% (p=1.3E-6) and 15.7% (p=3.6E-6) of the DMSO control treatment for MGPP6 and MGPP7, respectively. This dose was used throughout, similar to a study treating sarcoma cells with MK-1775 as a single agent at 500 nM ([30]). Treatment with MK-1775 effectively decreased levels of phosphorylation at CDK1 Y15, indicating on-target inhibition of Wee1, Figure 3D and Supplementary Figure S4B.

Mitotic Catastrophe and Apoptosis Induced after MK-1775 Treatment

To define the mechanism by which Wee1 kinase inhibition led to decreased cell counts, we used western blotting and flow cytometry to quantify DNA damage and DNA content following MK-1775 treatment. Intriguingly, as illustrated in Figure 4A and Supplementary Figure S5A, γH2AX, a marker of DNA damage ([31]), was strongly increased within 8 hours after cells were exposed to the drug, prior to any significant changes in total DNA content, Figure 4B and Supplementary Figure S5B, which were not detected until the 24 hour time point. This result suggests that these cells are under constant mutational stress and that Wee1 activity and CDK1 Y15 phosphorylation may be primarily responsible for inhibiting cell cycle progression during damage repair in this system. Increased DNA damage following MK-1775 treatment has a functional consequence, as we measured, using Hoechst staining, a significant increase in the percentage of cells with DNA content greater than 2N after treatment (p=1.6E-4 and p=1.5E-3 at 24 hours for MGPP6 and MGPP7, respectively), compared to the control, Supplementary Figure S5C and S5D.

Having documented a decrease in cell count, DNA damage pathway activation, and perturbation in cell cycle progression, we investigated induction of apoptosis by quantifying two apoptotic pathway markers, cleaved PARP ([32]) and cleaved Caspase-3 ([33]). There was a statistically significant increase in the percentage of cells expressing the cleaved forms of these proteins, as early as 24 hours after MK-1775 treatment (p=0.039 and p=0.042 for

MGPP6 cleaved PARP and cleaved Caspase-3, respectively; p=9.2E-3 and p=0.017 for MGPP7 cleaved PARP and cleaved Caspase-3, respectively); further increases in exposure time led to a greater effect, Figures 4C and 4D and Supplementary Figures S6A, S6B, and S6C.

To confirm that these results were due to inhibition of Wee1, we performed a rescue experiment in which cells were treated with roscovitine, a CDK inhibitor, MK-1775, or these two inhibitors for 24 hours. Roscovitine treatment alone had minimal effect on the cells. However, CDK inhibition by roscovitine effectively abrogated the increased DNA damage and altered DNA content caused by MK-1775, Figures 4E and 4F and Supplementary Figures S6D and S6E.

Confirmation of Results in GBM Patient-Derived Xenograft (PDX) Cell Lines

Induction of apoptosis with MK-1775 in primary cells derived from the engineered mouse model of proneural GBM led us to test our theory in a different GBM system, human GBM PDX tumors and cell lines ([13], [34]). We chose three PDX lines: GBM6, GBM36, and GBM38. All three are P53 mutated and GBM36 also has a homozygous deletion of PTEN. GBM36 has been subtyped as proneural, and GBM6 and GBM38 as classical, as defined by TCGA ([6]), Table 1.

Treatment of the PDX cell lines for 48 hours with 1μM MK-1775 led to a decrease in cell counts for all three lines, although the extent of the response varied, with GBM6 and GBM36 displaying increased sensitivity to MK-1775 compared to GBM38, Figure 5A. On-target inhibition of CDK1 phosphorylation, analyzed by western blot, reflected the phenotypic response, with decreased phospho-CDK1 as early as 8 hours in GBM6 and GBM36, and by 48 hours in GBM38, Figure 5B. Similar to the primary murine cell lines, all of the PDX model cell lines demonstrated activation of the DNA damage response pathway by 8 hours of treatment, Figure 5C.

To further characterize the PDX model cellular response to MK-1775, we used flow cytometry to quantify DNA content and apoptosis. Although minimal change in cellular DNA content was detected at 8 hours, there was a substantial increase in the population of cells that had a >2N DNA content after 48 hours of treatment, Figure 6A. Significant increases in cleaved PARP and cleaved Caspase-3 were also observed after 48 hours of treatment for all three cell lines, Figures 6B and 6C, again with the greatest increase occurring in GBM6.

PDX Flank Tumors Respond to MK-1775

After successfully inducing an apoptotic response and disruption of cell cycle arrest in cell culture, we tested MK-1775 treatment *in vivo* using a flank tumor PDX model, GBM6, as MK-1775 is poorly brain penetrant ([19]). A short-duration, 5 day, treatment study was used to assess molecular changes, while a long-duration treatment was used to investigate any changes in tumor growth after treatment with MK-1775.

In the short-duration study, 4 tumors (2 vehicle control and 2 MK-1775 treated) were analyzed for phospho- and total CDK1 and for γ-H2AX. Although the two MK-1775 treated

tumors had similar total CDK1 expression compared to the two vehicle treated tumors, their phospho-CDK1 levels were substantially decreased, Figure 7A. Tumors treated with MK-1775 also demonstrated increased γ-H2AX.

The long-duration *in vivo* study evaluated the effects of MK-1775 on tumor growth. There was a significant increase in time to endpoint (log-rank p=0.02) with MK-1775 treatment, Figure 7B. The average survival time after treatment initiation was 22 days with MK-1775 treatment and only 13 days with control. The tumor volume data was binned into three day increments, Figure 7C, which averages the day-to-day variation and allows better visualization of the stratification of treatment. These results demonstrate the applicability of MK-1775 as a monotherapy for *in vivo* tumors and suggest that suppression of Wee1 activity might be an effective strategy for P53-deficient GBM tumors expressing high CDK1 phosphorylation.

DISCUSSION

To identify novel intervention points in GBM tumor-specific signaling networks, we compared the phosphotyrosine signaling of 14 proneural GBM murine tumors to 8 murine brain controls and found vastly different signaling between the two tissue types.

Even using tumor homogenates, which inevitably includes a portion of cells from the local environment that are non-neoplastic, we have still demonstrated significant differences in signaling at the population level between tumors and brain. Reduced glutamate receptor phosphorylation, previously observed in GBM ([35, 36]), along with decreased phosphorylation of Dlg 2 (PSD-93), 3, and 4 (PSD-95) ([37]), and other neuron-specific proteins in our tumors likely reflect the differences in cellular composition between glioma and normal brain tissue ([21]). By comparison, phosphorylation of proteins involved in canonical oncogenic signaling networks, including ERK1/2 MAP kinases (T183/Y185 and T203/Y205 in the activation loop), PI3K regulatory subunit P85a, PDGFRα, and RTK scaffolds GAB1 and SHC, and cell cycle regulation (CDK1) were all increased in the tumor samples. Notably, our deconvolution analysis of RNA-Seq data shows that the genes encoding these phosphoproteins are predominantly or exclusively expressed in olig2+ cells. Although many of the other phosphorylation sites that were increased in the tumor tissues have not been implicated specifically in PDGFRα signaling or tumor growth, several of these sites are on proteins that have been associated with increased tumor progression, Supplementary Table S1. Our data confirm the presence of specific sites on these proteins in tumor tissues; the functional consequence of increased phosphorylation of these sites in these tissues remains to be determined.

The phosphorylation site that was most increased in the tumor tissues was on the cell cycle regulator, CDK1 pY15. CDK1 Y15 phosphorylation by the Wee1 kinase holds the protein in an inactive state until the DNA is fully replicated and any necessary DNA repair is completed ([29]). Cyclins and CDKs allow cell cycle transitions in a unidirectional and tightly controlled manner. The P53 tumor suppressor is an upstream inhibitor of cyclins after DNA damage, causing cell cycle arrest primarily in G1, but also in G2 ([8–10]). In the presence of TP53 mutations or deletions, such as in our genetically engineered proneural tumors, cells

may be able to progress through the cell cycle with DNA damage, depending on the status of other cell cycle checkpoints. Hence, in these cells Wee1 phosphorylation of CDK1 at tyrosine 15 may be critical to inhibit cell entry into mitosis after DNA damage ([38]).

Previous studies have demonstrated the efficacy of inhibiting Wee1 in combination with DNA damaging agents, such as gemcitabine ([39–42]) in the context of non-functional P53. MK-1775 monotherapy has been previously documented by Kreahling et al. ([30]) where tumor explants treated with 500 nM MK-1775 for 24 hours demonstrated decreased CDK1 phosphorylation and features of cell death. Building on these results, here we have used multiple tumor derived cell lines and a flank PDX model to assess the effectiveness of monotherapy with MK-1775 in in vitro and in vivo models of GBM with a range of characteristics, Table 1. Following exposure to MK-1775, tumor derived human and murine cell lines experience DNA damage, have deregulated cell cycle progression, and die by apoptosis, suggesting they either undergo mitotic catastrophe or S-phase arrest and cell death, independent of their GBM subtype or specific molecular characteristics. Intriguingly, even without the addition of an exogenous DNA-damaging agent, which has been often used in conjunction with MK-1775, we observed rapid and strong increases in γH2AX and decreased cell number after treatment compared with the control. These models were all P53 independent, removing a G1-S checkpoint ([8–10]), possibly paving the way for this therapy to be effective in cells and tumors that are more dependent on cell cycle checkpoints later in the cell cycle.

Perhaps not surprisingly, there was greater variability across the PDX models derived from three different patients, Table 1, compared to the syngeneic murine models. Relative to the other PDX models, GBM38 demonstrated an increased cell count after 48 hours of 1μM MK-1775 and we observe a corresponding decreased phosphorylation of CDK1. Although the percentage of GBM38 cells in S/G2/M increased after 48 hours of treatment, G1 (2N) was still the dominant peak in the histogram, unlike the other two cell lines that have more similar percentages of cells in G1 and G2/M. This effect could be due to a reduced sensitivity of GBM38 to MK-1775 or a slower proliferation rate of GBM38 relative to the other models. These endpoints complement each other and highlight the “patient” specific effect of treatment. It is worth noting that the methylation status of these PDX tumors has previously been shown to correlate to the primary tumors from which they were derived ([34]), therefore suggesting extensibility of Wee1 inhibition from the mouse and PDX models to human GBM, even across varied molecular backgrounds.

Finally, we tested the effect of monotherapy MK-1775 in vivo on flank PDX GBM6 tumors. Flank PDX tumors exposed to MK-1775 demonstrated decreased phosphorylation of CDK1 Y15 and increased DNA damage. Treatment with the inhibitor slowed tumor growth and led to a 1.74-fold improvement in time to exceed tumor size endpoints, while treatment with temozolomide in a previous study using this same PDX GBM6 model ([34]) demonstrated only a 1.39-fold improvement. Treating with a specific inhibitor as a single agent not only increases the anti-tumor benefit in this model, but would decrease off target effects of a general DNA damaging, O6-methylguanine lesion inducing agent such as temozolomide ([43]).

Here we have demonstrated the utility of quantitative phosphoproteomics to highlight signaling networks significantly enhanced in tumor tissues relative to their normal tissue counterparts and reveal potential therapeutic targets. Although in this study we have focused on the effect of inhibiting Wee1 due to the strong increase in phosphorylation of CDK1 in the tumor tissues, there are many other altered phosphorylation sites in these tissues that may represent additional targets, potentially in combination with Wee1 inhibition. Further investigation of these sites in this model and others may lead to improved therapy for this disease.

Supplementary Material

Refer to Web version on PubMed Central for supplementary material.

Acknowledgments

Financial Support

This work was supported by NIH grants CA112967 (F.M. White), CA159988 (F.M. White), CA014051 (F.M. White), ES007020 (F.M. White), EB016071 (P.A. Sims), NS073610 (P. Canoll), and NS066955 (P. Canoll), CA184320 (J.N. Sarkaria), and Mayo Clinic (J.N. Sarkaria), the Mayo Brain Tumor SPORE CA108961 (J.N. Sarkaria), and Brain Tumor Ecology Collaborative funding from the James S. McDonnell Foundation (P. Canoll and P.A. Sims).

REFERENCES

1. Ostrom QT, Gittleman H, Farah P, Ondracek A, Chen Y, Wolinsky Y, et al. CBTRUS Statistical Report : Primary Brain and Central Nervous System Tumors Diagnosed in the United States in 2006 – 2010. Neuro-Oncology. 2013; 15:ii1–ii56. [PubMed: 24137015]
2. Stupp R, Hegi ME, Mason WP, van den Bent MJ, Taphoorn MJ, Janzer RC, et al. Effects of radiotherapy with concomitant and adjuvant temozolomide versus radiotherapy alone on survival in glioblastoma in a randomised phase III study: 5-year analysis of the EORTC-NCIC trial. Lancet Oncol. 2009; 10:459–466. [PubMed: 19269895]
3. Furnari FB, Fenton T, Bachoo RM, Mukasa A, Stommel JM, Stegh A, et al. Malignant astrocytic glioma: Genetics, biology, and paths to treatment. Genes Dev. 2007; 21:2683–2710. [PubMed: 17974913]
4. McLendon R, Friedman A, Bigner D, Van Meir EG, Brat DJM, Mastrogianakis G, et al. Comprehensive genomic characterization defines human glioblastoma genes and core pathways. Nature. 2008; 455:1061–1068. [PubMed: 18772890]
5. Brennan CW, Verhaak RGW, McKenna A, Campos B, Noushmehr H, Salama SR, et al. The Somatic Genomic Landscape of Glioblastoma. Cell. 2013; 155:462–477. [PubMed: 24120142]
6. Verhaak RGW, Hoadley KA, Purdom E, Wang V, Qi Y, Wilkerson MD, et al. Integrated Genomic Analysis Identifies Clinically Relevant Subtypes of Glioblastoma Characterized by Abnormalities in PDGFRA, IDH1, EGFR, and NF1. Cancer Cell. 2010; 17:98–110. [PubMed: 20129251]
7. Patel AP, Tirosh I, Trombetta JJ, Shalek AK, Gillespie SM, Wakimoto H, et al. Single-cell RNA-seq highlights intratumoral heterogeneity in primary glioblastoma. Science. 2014; 344:1396–1401. [PubMed: 24925914]
8. Agarwal ML, Agarwal A, Taylor WR, Stark GR. p53 controls both the G2/M and the G1 cell cycle checkpoints and mediates reversible growth arrest in human fibroblasts. Proc Natl Acad Sci U S A. 1995; 92:8493–8497. [PubMed: 7667317]
9. Bunz F, Dutriaux A, Lengauer C, Waldman T, Zhou S, Brown JP, et al. Requirement for p53 and p21 to sustain G2 arrest after DNA damage. Science. 1998; 282:1497–1501. [PubMed: 9822382]

10. Goi K, Takagi M, Iwata S, Delia D, Asada M, Donghi R, et al. DNA damage-associated dysregulation of the cell cycle and apoptosis control in cells with germ-line p53 mutation. Cancer Res. 1997; 57:1895–1902. [PubMed: 9157982]
11. Lei L, Sonabend AM, Guarnieri P, Soderquist C, Ludwig T, Rosenfeld S, et al. Glioblastoma models reveal the connection between adult glial progenitors and the proneural phenotype. PLoS One. 2011; 6:30–32.
12. Carlson BL, Pokorny JL, Schroeder MA, Sarkaria JN. Establishment, Maintenance, and In Vitro and In Vivo Applications of Primary Human Glioblastoma Multiforme (GBM) Xenograft Models for Translational Biology Studies and Drug Discovery. Current Protocols in Pharmacology. 2011; 52(14.16):1–23.
13. Sarkaria JN, Carlson BL, Schroeder Ma, Grogan P, Brown PD, Giannini C, et al. Use of an orthotopic xenograft model for assessing the effect of epidermal growth factor receptor amplification on glioblastoma radiation response. Clin Cancer Res. 2006; 12:2264–2271. [PubMed: 16609043]
14. Johnson H, White FM. Quantitative Analysis of Signaling Networks across Differentially Embedded Tumors Highlights Interpatient Heterogeneity in Human Glioblastoma. J Proteome Res. 2014; 13:4581–4593. [PubMed: 24927040]
15. Johnson H, Lescarbeau RS, Gutierrez JA, White FM. Phosphotyrosine profiling of NSCLC cells in response to EGF and HGF reveals network specific mediators of invasion. J Proteome Res. 2013; 12:1856–1867. [PubMed: 23438512]
16. Zhang Y, Wolf-Yadlin A, Ross PL, Pappin DJ, Rush J, Lauffenburger Da, et al. Time-resolved mass spectrometry of tyrosine phosphorylation sites in the epidermal growth factor receptor signaling network reveals dynamic modules. Mol Cell Proteomics. 2005; 4:1240–1250. [PubMed: 15951569]
17. Arneja A, Johnson H, Gabrovsek L, Lauffenburger DA, White FM. Qualitatively Different T Cell Phenotypic Responses to IL-2 versus IL-15 Are Unified by Identical Dependences on Receptor Signal Strength and Duration. J Immunol. 2013; 192:123–135. [PubMed: 24298013]
18. Curran TG, Bryson BD, Reigelhaupt M, Johnson H, White FM. Computer aided manual validation of mass spectrometry-based proteomic data. Methods. 2013; 61:219–226. [PubMed: 23500044]
19. Pokorny JL, Calligaris D, Gupta SK, Iyekegbe DO, Mueller D, Bakken KK, et al. The efficacy of the Wee1 inhibitor MK-1775 combined with temozolomide is limited by heterogeneous distribution across the blood-brain barrier in glioblastoma. Clin Cancer Res. 2015; 21(8):1916–1924. [PubMed: 25609063]
20. Sonabend AM, Bansal M, Guarnieri P, Lei L, Amendolara B, Soderquist C, et al. The transcriptional regulatory network of proneural glioma determines the genetic alterations selected during tumor progression. Cancer Res. 2014; 74:1440–1451. [PubMed: 24390738]
21. Gill BJ, Pisapia DJ, Malone HR, Goldstein H, Lei L, Sonabend A, et al. MRI-localized biopsies reveal subtype-specific differences in molecular and cellular composition at the margins of glioblastoma. Proc Natl Acad Sci. 2014; 111(34):12550–12555. [PubMed: 25114226]
22. Gonzalez C, Sims JS, Hornstein N, Mela A, Garcia F, Lei L, et al. Ribosome Profiling Reveals a Cell-Type Specific Translational Landscape in Glioma. J. Neuroscience. 2014; 34:10924–10936. [PubMed: 25122893]
23. Best DJ, Roberts DE. Algorithm AS 89: The Upper Tail Probabilities of Spearman's Rho. J. Royal Stat Society, Series C (Applied Stat). 1975; 24(3):377–379.
24. Heldin CH, Ostman a, Rönnstrand L. Signal transduction via platelet-derived growth factor receptors. Biochim Biophys Acta. 1998; 1378:F79–F113. [PubMed: 9739761]
25. Carracedo A, Pandolfi PP. The PTEN-PI3K pathway: of feedbacks and cross-talks. Oncogene. 2008; 27:5527–5541. [PubMed: 18794886]
26. Boulton TG, Cobb MH. Identification of multiple extracellular signal-regulated kinases (ERKs) with antipeptide antibodies. Cell Regul. 1991; 2:357–371. [PubMed: 1654126]
27. Wolf I, Rubinfeld H, Yoon S, Marmor G, Hanoch T, Seger R. Involvement of the Activation Loop of ERK in the Detachment from Cytosolic Anchoring. J Biol Chem. 2001; 276:24490–24497. [PubMed: 11328824]

28. Himanen JP, Saha N, Nikolov DB. Cell-cell signaling via Eph receptors and ephrins. Curr Opin Cell Biol. 2007; 19:534–542. [PubMed: 17928214]
29. Perry JA, Kornbluth S. Cdc25 and Wee1: analogous opposites? Cell Div. 2007; 2:12. [PubMed: 17480229]
30. Kreahling JM, Gemmer JY, Reed D, Letson D, Bui M, Altiok S. MK1775, a Selective Wee1 Inhibitor, Shows Single-Agent Antitumor Activity against Sarcoma Cells. Mol Cancer Ther. 2011; 11:174–182. [PubMed: 22084170]
31. Rogakou EP, Pilch DR, Orr aH, Ivanova VS, Bonner WM. Double-stranded Brekas Induce Histone H2AX phosphorylation on Serine 139. J Biol Chem. 1998; 273:5858–5868. [PubMed: 9488723]
32. Kaufmann SH, Desnoyers S, Ottaviano Y, Apoptosis C, Davidson NE, Poirier GG. Specific Proteolytic Cleavage of Poly (ADP-ribose) Polymerase : An Early Marker of Chemotherapy-induced Apoptosis Specific Proteolytic Cleavage of Poly (ADP-ribose) Polymerase : An Early Marker of. Cancer Res. 1993; 53:3976–3985. [PubMed: 8358726]
33. Janicke RU. Caspase-3 Is Required for DNA Fragmentation and Morphological Changes Associated with Apoptosis. J Biol Chem. 1998; 273:9357–9360. [PubMed: 9545256]
34. Carlson BL, Grogan PT, Mladek AC, Schroeder M a, Kitange GJ, Decker Pa, et al. Radiosensitizing Effects of Temozolomide Observed in vivo only in a Subset of O6-Methylguanine-DNA Methyltransferase Methylated Glioblastoma Multiforme Xenografts. Int J Radiat Oncol Biol Phys. 2009; 75:212–219. [PubMed: 19695438]
35. van Vuurden DG, Yazdani M, Bosma I, Broekhuizen aJF, Postma TJ, Heimans JJ, et al. Attenuated AMPA receptor expression allows glioblastoma cell survival in glutamate-rich environment. PLoS One. 2009; 4(6):e5953. [PubMed: 19536293]
36. Markert JM, Fuller CM, Gillespie GY, Bubien JK, McLean La, Hong RL, et al. Differential gene expression profiling in human brain tumors. Physiol Genomics. 2001; 5:21–33. [PubMed: 11161003]
37. Brenman JE, Christopherson KS, Craven SE, McGee AW, Bredt DS. Cloning and characterization of postsynaptic density 93, a nitric oxide synthase interacting protein. J Neurosci. 1996; 16:7407–7415. [PubMed: 8922396]
38. McGowan CH, Russell P. Cell cycle regulation of human WEE1. EMBO J. 1995; 14:2166–2175. [PubMed: 7774574]
39. Rajeshkumar NV, De Oliveira E, Ottenhof N, Watters J, Brooks D, Demuth T, et al. MK-1775, a potent Wee1 inhibitor, synergizes with gemcitabine to achieve tumor regressions, selectively in p53-deficient pancreatic cancer xenografts. Clin Cancer Res. 2011; 17:2799–2806. [PubMed: 21389100]
40. Aarts M, Sharpe R, Garcia-Murillas I, Gevensleben H, Hurd MS, Shumway SD, et al. Forced mitotic entry of S-phase cells as a therapeutic strategy induced by inhibition of WEE1. Cancer Discov. 2012; 2:524–539. [PubMed: 22628408]
41. Hirai H, Arai T, Okada M, Nishibata T, Kobayashi M, Sakai N, et al. MK-1775, a small molecule Wee1 inhibitor, enhances antitumor efficacy of various DNA-damaging agents, including 5-fluorouracil. Cancer Biol Ther. 2010; 9:514–522. [PubMed: 20107315]
42. Sarcar B, Kahali S, Prabhu aH, Shumway SD, Xu Y, Demuth T, et al. Targeting Radiation-Induced G2 Checkpoint Activation with the Wee-1 Inhibitor MK-1775 in Glioblastoma Cell Lines. Mol Cancer Ther. 2011; 10:2405–2414. [PubMed: 21992793]
43. Roos WP, Batista LFZ, Naumann SC, Wick W, Weller M, Menck CFM, et al. Apoptosis in malignant glioma cells triggered by the temozolomide-induced DNA lesion O6-methylguanine. Oncogene. 2007; 26:186–197. [PubMed: 16819506]

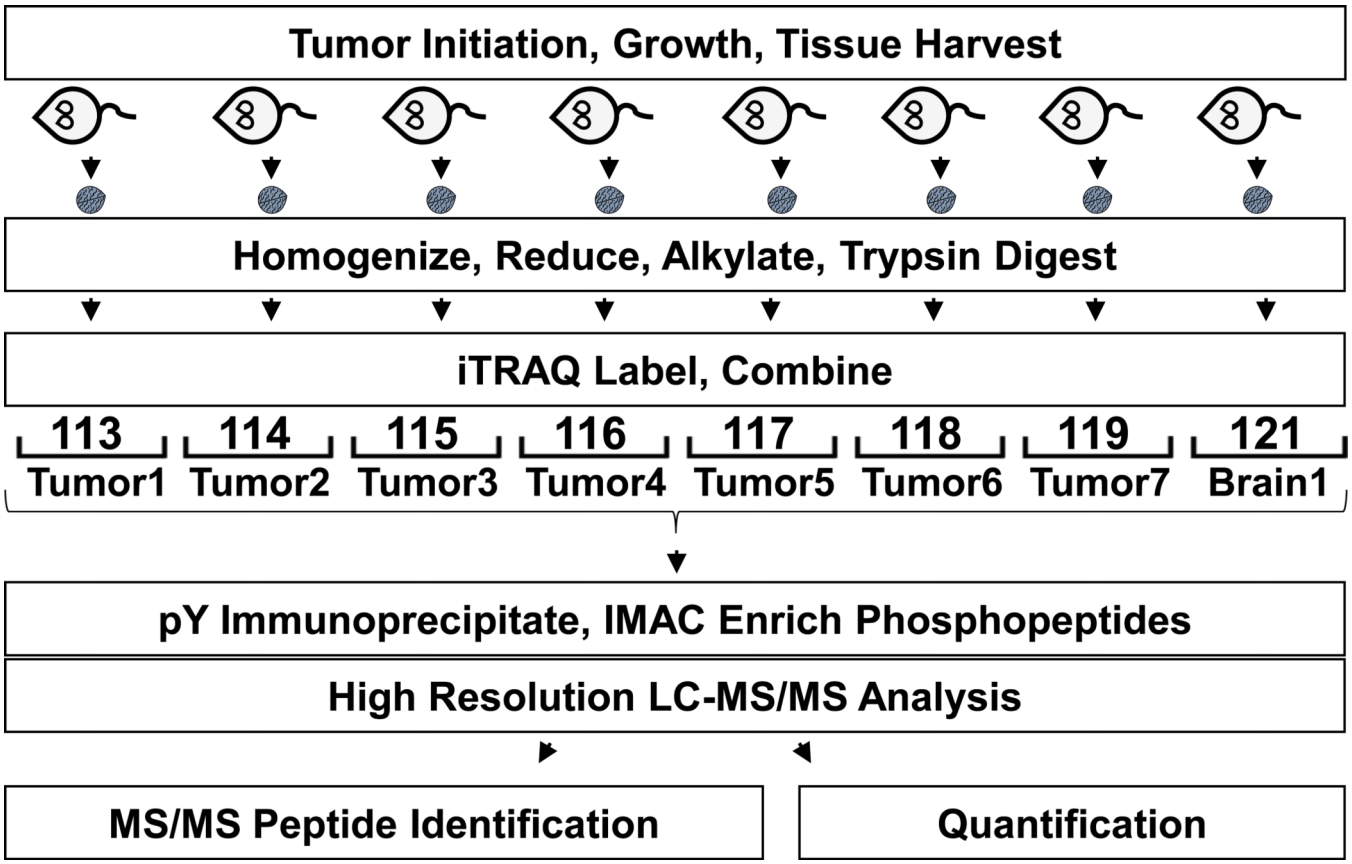

Figure 1.

Schematic diagram of the mass spectrometry experimental workflow. Tumors were initiated by a retroviral injection and tumors grew until mice demonstrated morbidity. The mice were anaesthetized and tumors or brain tissues were excised and immediately flash frozen. Tissue samples were homogenized and proteins were reduced, alkylated, and digested with trypsin. Peptides were differentially labeled with iTRAQ, and phosphotyrosine peptides were enriched using peptide IP and IMAC. Phosphotyrosine peptides were then analyzed by LC-MS/MS. Peptide fragmentation generated sequence specific ions, enabling identification of the phosphosite (left) and iTRAQ marker ions (right), providing quantification of the phosphopeptide levels across the various biological samples.

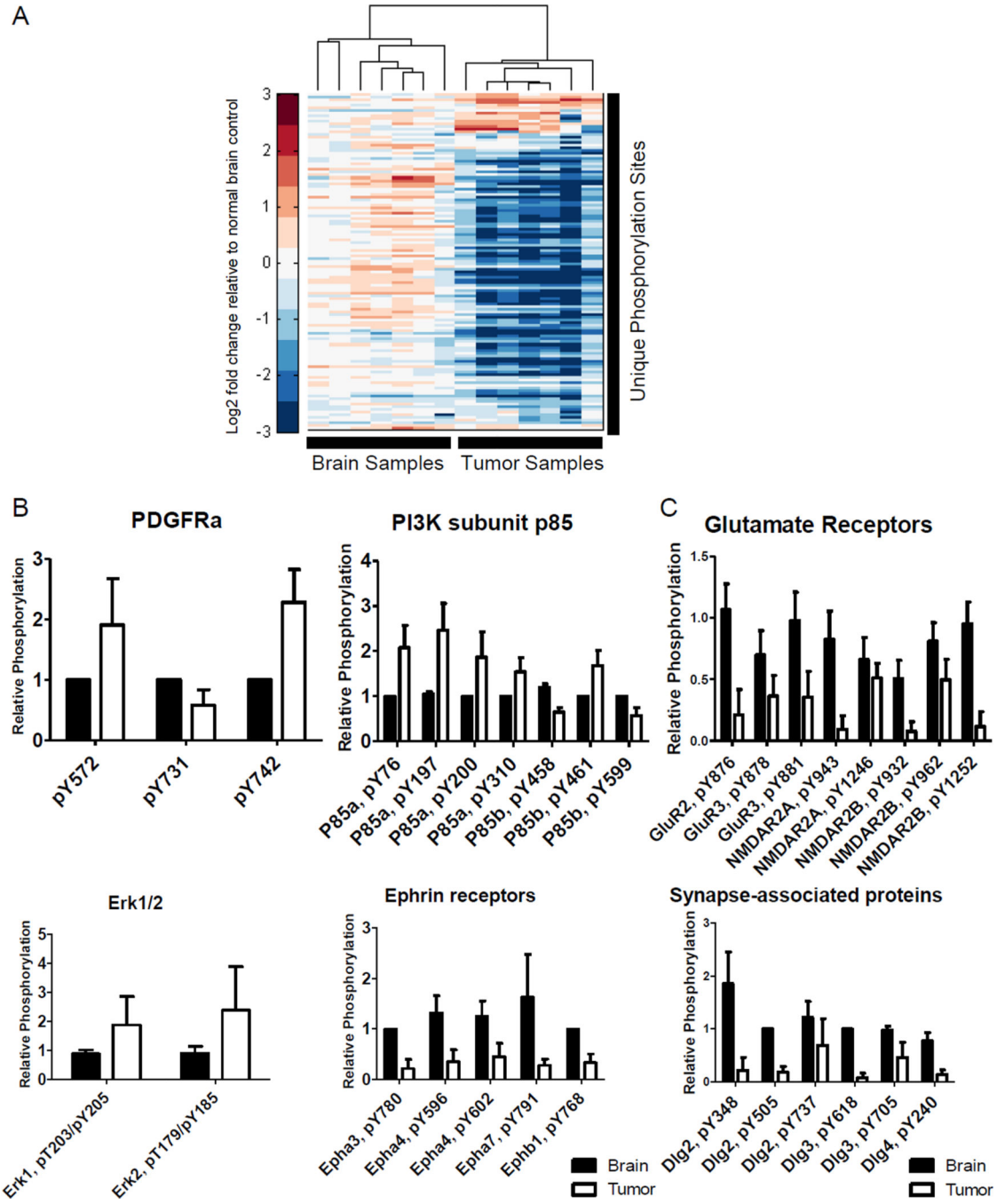

Figure 2.

Global and specific differences between tumors and brain samples. A. Heatmap of the 125 phosphopeptides quantified in both analyses. iTRAQ quantification is reported as fold changes normalized to one brain sample present in both analyses and log2 transformed. Phosphorylation sites were hierarchically clustered. B. iTRAQ quantification of phosphotyrosine sites on PDGFRα, PI3K subunit P85, Erk1 and Erk2, and ephrin receptors in tumors and brain tissues relative to brain control. C. iTRAQ quantification of

phosphotyrosine sites on glutamate receptors and synapse-associated proteins in tumors and brain tissues relative to a brain control.

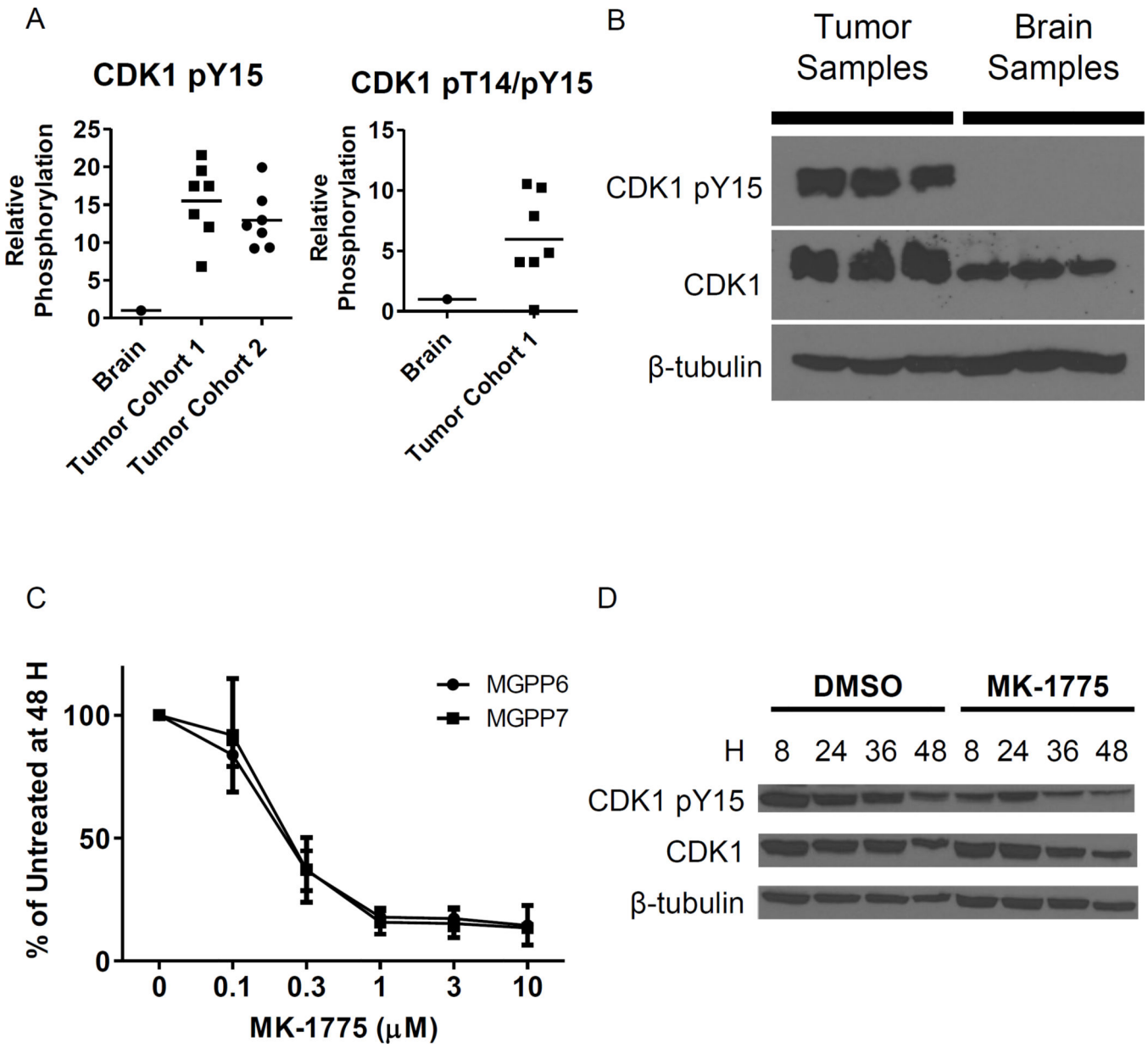

Figure 3.

CDK1 phosphorylation in murine tumors and primary cell lines. A. iTRAQ quantification of singly (pY15) and doubly phosphorylated (pT14/pY15) CDK1 in two and one cohort(s), respectively, relative to the brain control. Samples are represented by the following symbols: Tumor Cohort 1 (■), Tumor Cohort 2 (▲), and Brain Control (●). B. Immunoblotting of CDK1 pY15, CDK1, and β-tubulin used as a loading control for three tumors and three brain samples. Each sample is a unique biological tissue sample. C. Cell counts at 48 hours of MGPP6 (●) and MPGG7 (■) primary murine GBM cell lines in response to MK-1775 treatment at the indicated concentrations, normalized to the DMSO control. D. Immunoblotting of CDK1 pY15, CDK1, and the loading control β-tubulin of the MGPP6 cell line after treatment with 1μM MK-1775 or DMSO for the indicated lengths of time.

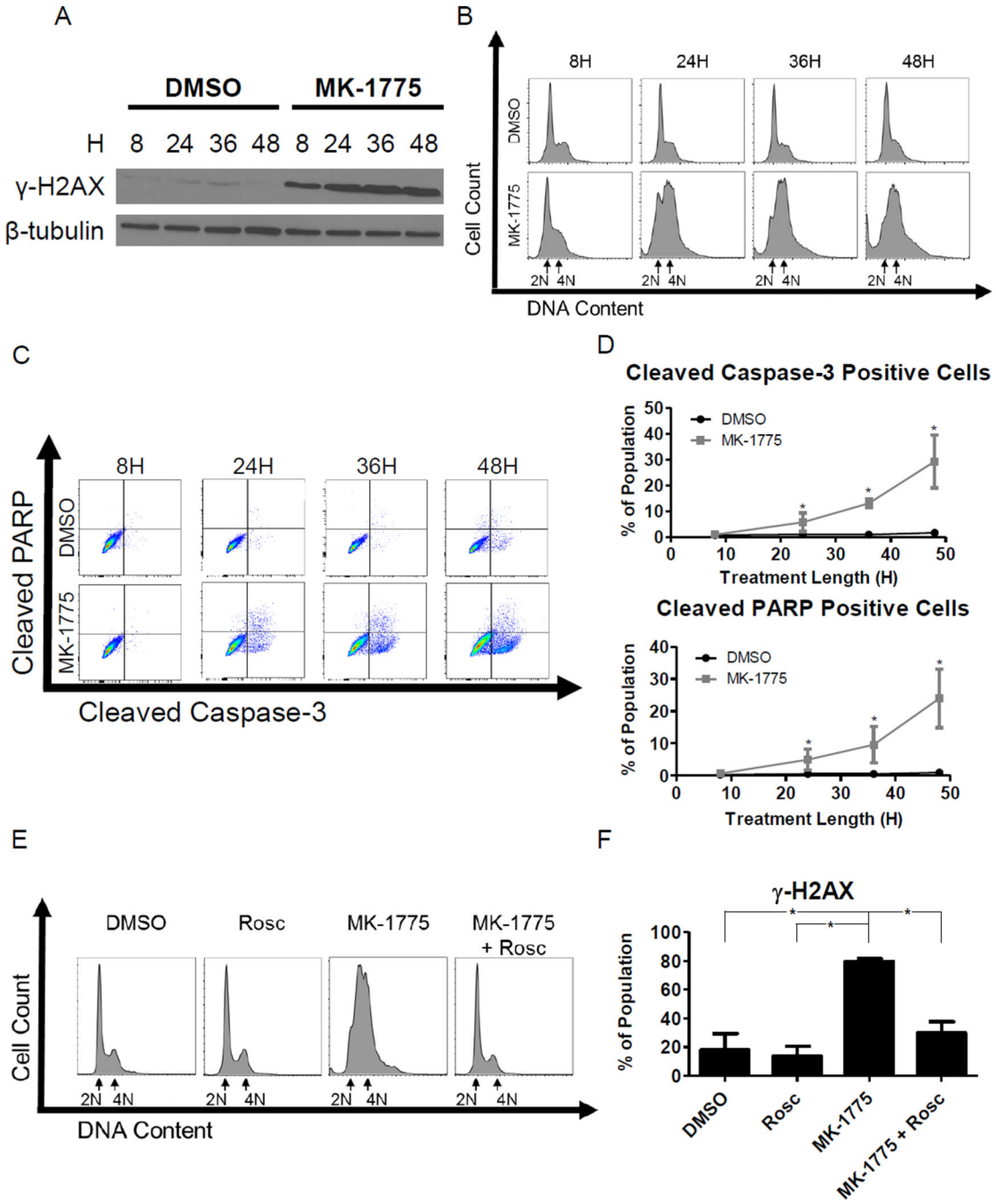

Figure 4.

MK-1775 causes primary cells to undergo mitotic catastrophe and apoptosis. A. Immunoblotting of γH2AX and the loading control β-tubulin of the MGPP6 cell line after treatment with 1μM MK-1775 or DMSO for the indicated lengths of time. B. DNA content histogram of MGPP6 after treatment with 1μM MK-1775 or DMSO for the indicated lengths of time with 2N and 4N chromosomal content indicated. C. Representative bivariate dot plot of MGPP6 cells treated with 1μM MK-1775 or DMSO for the indicated lengths of time. The vertical axis shows anti-cleaved PARP staining and the horizontal axis shows anti-cleaved

Caspase-3 staining. The quadrants are set from the DMSO 8 hour control. D. Quantification of cleaved PARP positive and cleaved Caspase-3 positive MGPP6 cells after treatment with 1μM MK-1775 (■) or DMSO (●). E and F. MGPP6 DNA content histogram with 2N and 4N chromosomal content indicated and γH2AX positive cells, respectively, after treatment with DMSO, 10μM roscovitine (Rosc), 1μM MK-1775, or 1μM MK-1775 and 10μM Rosc for 24 hours. * indicates $p<0.05$.

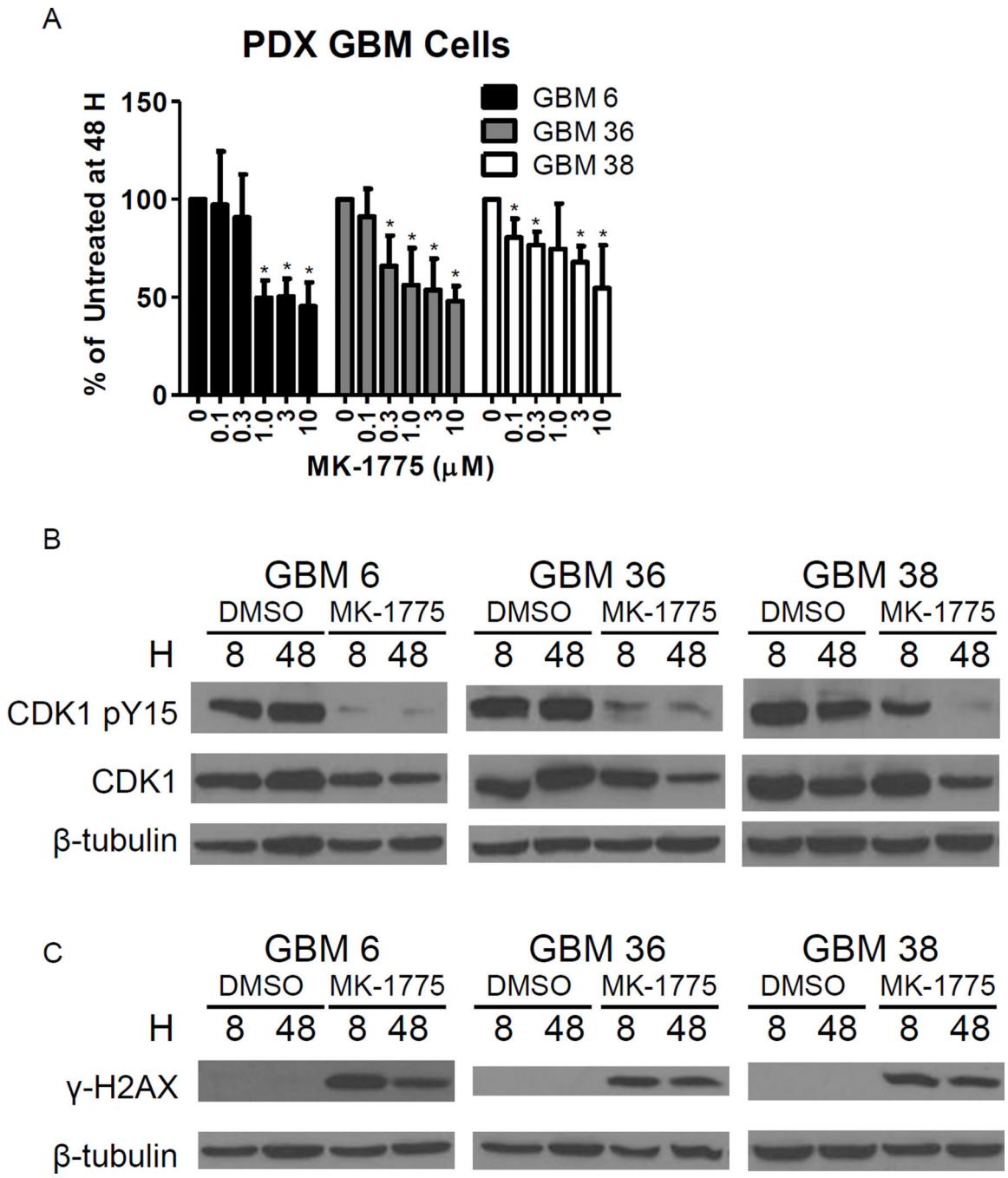

Figure 5.

GBM PDX models' responses to MK-1775. A. Cell count of three GBM PDX models, GBM6, GBM36, and GBM38, after treatment with MK-1775 at the indicated concentrations for 48 hours. All measurements are relative to the DMSO control. * indicates $p<0.05$. B. Immunoblotting of CDK1 pY15, CDK1, and the loading control β-tubulin for the three PDX models after 8 and 48 hours of treatment of 1μM MK-1775 or DMSO. C. Immunoblotting of γH2AX and the loading control β-tubulin for the three PDX models after 8 and 48 hours of treatment of 1μM MK-1775 or DMSO.

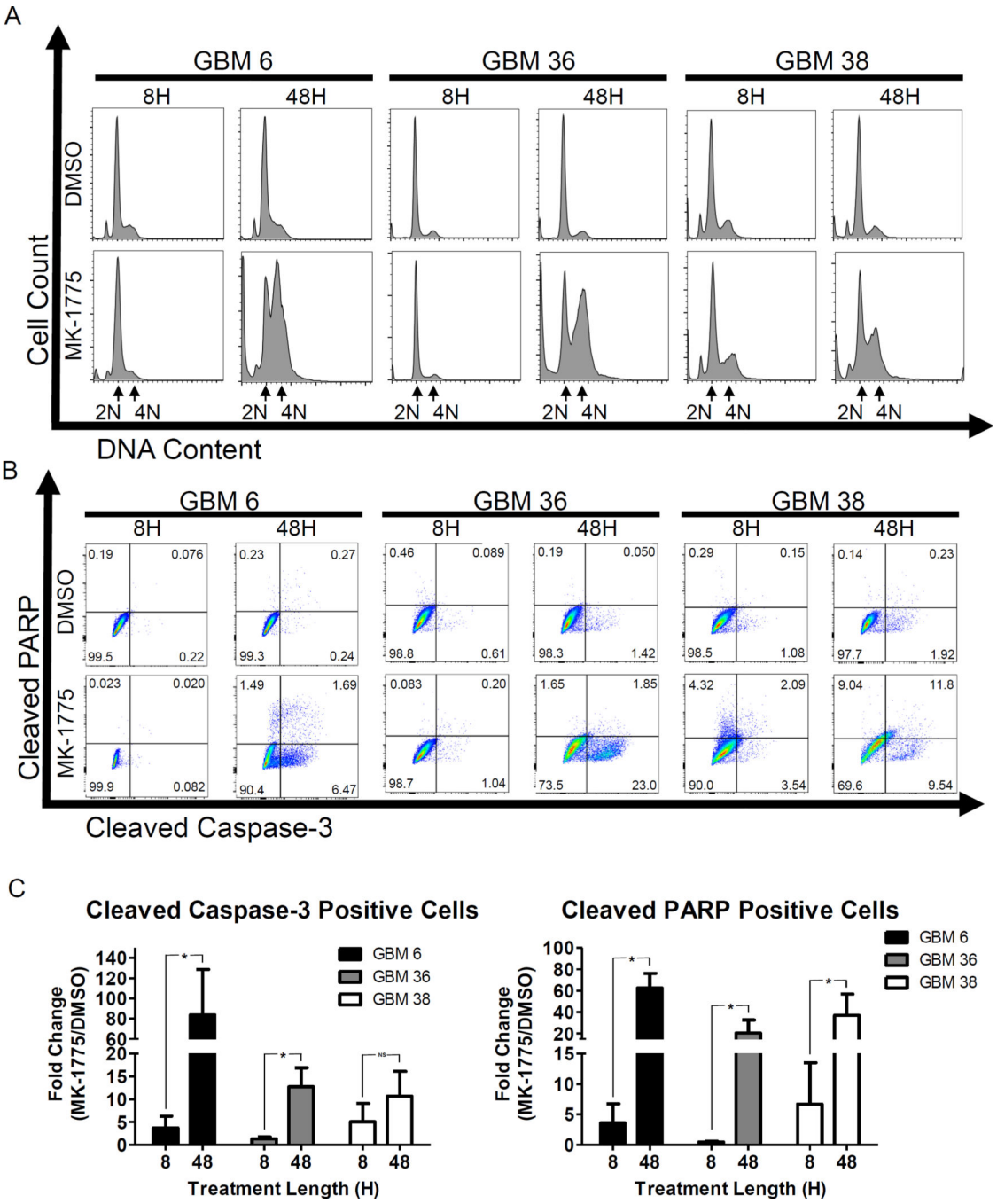

Figure 6.

Altered DNA content and apoptotic markers in MK-1775 treated PDX cells. A. DNA content histogram of GBM6, GBM36, and GBM38 after 1μM MK-1775 or DMSO for 8 or 48 hours of treatment with 2N and 4N chromosomal content indicated. B. Representative bivariate dot plot of GBM6, GBM36, and GBM38 cells after 1μM MK-1775 or DMSO treatment for 8 or 48 hours. The vertical axis shows anti-cleaved PARP staining and the horizontal axis shows anti-cleaved Caspase-3 staining. The quadrants are set from the DMSO 8 hour control. C. Fold change of the percentage of cleaved PARP positive and

cleaved Caspase-3 positive cells after treatment with 1μM MK-1775 for 8 or 48 hours relative to DMSO control.

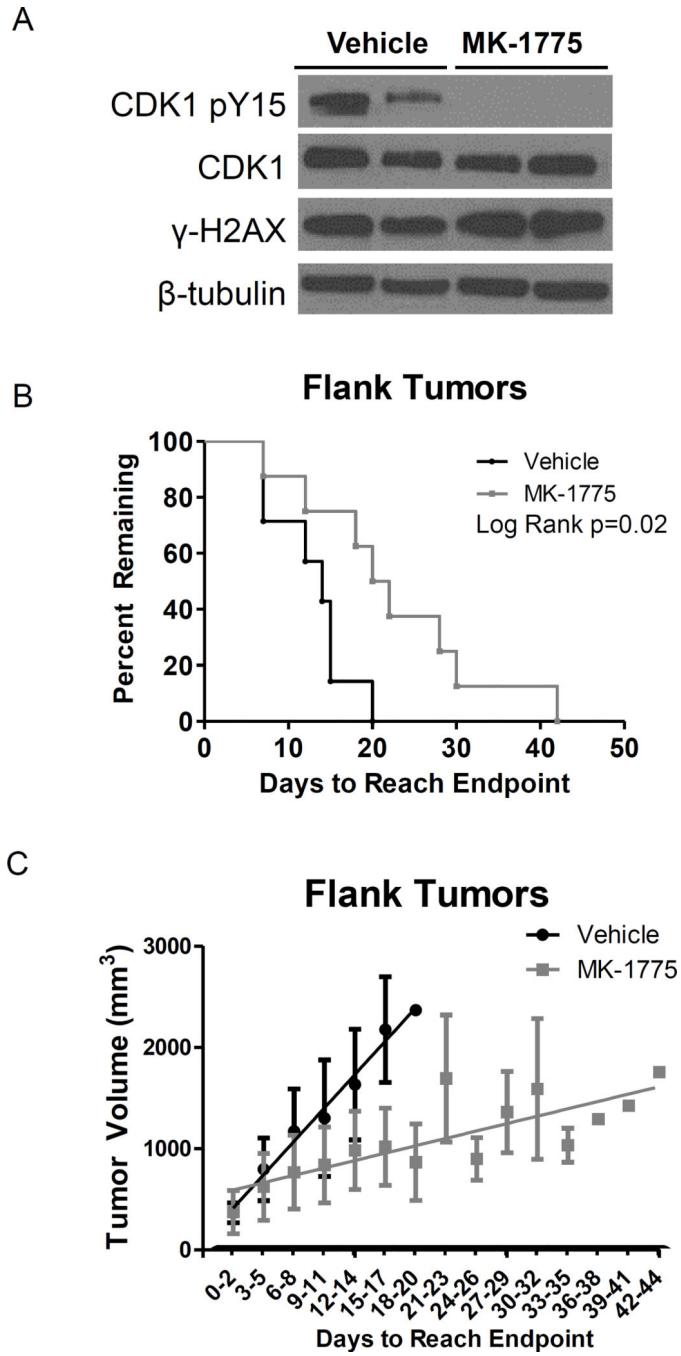

Figure 7.

Flank PDX tumors respond to MK-1775. A. Immunoblotting of CDK1 pY15, CDK1, γH2AX, and the loading control β-tubulin of tumors from MK-1775 and vehicle-control treated mice. Mice with established tumors were treated orally for 5 days and then the tumors were excised and analyzed. B and C. Mice with established flank tumors were randomized and treated with either MK-1775 (■, n=8) or vehicle (●, n=7) until tumors exceeded 1500 mm^3 twice or 2000 mm^3 once. Kaplan-Meier plot is shown in B, log-rank

p=0.02. The average tumor volume of tumors measured within each three day window after treatment begins are shown in C.

Table 1

Patient and Molecular Characteristics of the GBM PDX Models.

	Donor Characteristics					Molecular Characteristics				
	Age(Y) /Sex	**Tumor Location**	**Diagnosis**	**Time To Progression (mo)**	**Survival (mo)**	**GBM Subtype**	**PTEN status**	**p53 mutation**	**p16 deletion**	**EGFR amplification**
GBM 6	65/M	Frontal	Glioblastoma	5	16	Classical	WT	273: arg>cys	Yes	Yes, VIII
GBM 36	53/M	Cerebellum	Glioblastoma	2	10	Proneural	Homozygous Deletion	132: lys>met	Yes	No
GBM 38	71/F	Temporal	Glioblastoma	3	11, alive	Classical	WT	110: arg>cys	Yes	Yes, WT

Adapted with permission from from Carlson et al. 2011, Current Protocols in Pharmacology, copyright 2011 John Wiley & Sons, Inc ([12]) and Sarkaria et al. 2006, Clinical Cancer Research, copyright 2006 American Association for Cancer Research ([13]). Tumors were classified by GBM subtype as defined by TCGA ([6]).